A Baseband Wireless VNA for the Characterization of Multi-Port Distributed Systems

A Baseband Wireless VNA for the Characterization of Multi-Port Distributed Systems

Markeljan Fishta, *Member, IEEE*, Erica Raviola, *Member, IEEE*, and Franco Fiori, *Member, IEEE*

***Abstract*—Frequency characterization of spatially-large structures has become increasingly required, mostly in the fields of Structural Health Monitoring and Communication Systems based on non conventional media. When the ports of the system under measurement are far apart, methods based on traditional wired instruments become unattractive for field applications, due to the increased complexity, cost and signal integrity related issues. Aiming towards removing the wired connection from the ports of the system under test and the elaboration unit, the main issue to be dealt with is the time-synchronization of measurements at the ports. This contribution proposes a solution to such an issue by presenting a Wireless Vector Network Analyzer, suitable for the characterization of distributed systems. For this purpose, a wireless synchronization scheme is proposed, which is based on the disciplining of the signal sampling clock from the 1-Pulse-Per-Second reference signal. The proposed synchronization method reduces clock jitter at different ports at $1.13\,\mu s$ over a $300\,s$ observation interval. The hardware and software implementation of the system are detailed and experimental results proving its operation are provided.**

***Index Terms*—Distributed measurement systems, frequency response, impedance measurement, network analyzers, sensors and actuators, time-domain measurements**

I. Introduction

FREQUENCY characterization of multi-port devices is commonly performed by means of Vector Network Analyzers (VNAs). With the device to be characterized having a distributed nature, meaning large physical dimensions, long cables are needed to wire the ports of the device to the VNA. As the physical dimensions of the system increase, the complexity of the measurement setup increases as well.

The need for characterizing distributed systems arises in the frequency response measurement of non conventional communication channels [1], which is an important step in the process of designing and developing a communication system. The choice of modulation parameters like carrier frequency and data-rate is strongly related to the frequency response of the channel [1]–[4]. Another instance requiring the measurement of frequency response of objects with large physical dimensions is in Structural Health Monitoring (SHM) applications, when using the Transfer Impedance (TI) approach [5]–[10].

In such applications, the frequency characterization is performed by using transducers coupled to the structure under test, which are wired to traditional instruments [2], [5], [9] or custom hardware platforms [10], [11]. The wired solution, although reliable and precise, has the drawback of being complex and expensive, resulting not attractive for field applications. Moreover, long cables can give rise to signal integrity issues, picking up disturbances and noise [12]. This means that much effort has to be put into grounding and shielding related issues, further increasing system cost.

Traditional VNAs perform magnitude and phase measurements, which is only possible when the same timebase is used for the port signals. This is accomplished by synchronous acquisition, enabled by the wired connection of the VNA to the system under test. Instead, wanting to remove the wires between the network ports and the VNA central unit, the main challenge is the precise time-synchronization of the signal acquisition at the ports. With respect to such challenge, previous works have proposed various solutions, although none of them were aimed to address the transfer function measurement problem. Existing works are situated mainly in the SHM field, where acquisition among different sensors must have a time deviation lower than $120\,\mu s$ in order for the SHM techniques to be effective [13].

For instance, [14] proposed a synchronization scheme among a large number of sensors, based on two levels. Synchronization at the higher level, among few nodes, was performed by means of a timing signal received from the Global Positioning System (GPS), which is known as 1-Pulse-Per-Second (1PPS). These nodes, named coordinators, govern clusters of other sensing nodes and synchronize them through a beacon sending scheme. The reported worst case timing error between two sensor nodes was of $\pm 23\,\mu s$, which means that two nodes can have clocks differing of $\Delta t_{\mathrm{MAX}} = 46\,\mu s$. Such a time error is acceptable for the identification of mode shapes but, if transfer functions are to be measured, a large phase error can result. Indeed, assuming a typical frequency range for the considered applications [10] with an upper bound $f_{\mathrm{MAX}} = 2\,\mathrm{kHz}$, the resulting phase error can be as large as $\Delta\varphi = 360° \cdot f_{\mathrm{MAX}} \cdot \Delta t_{\mathrm{MAX}} = 33.12°$.

In [15] a hardware-based synchronization system for WSNs was proposed. The system, based on the nodes receiving a disciplining signal from a master unit, reported very low spatial jitter among the nodes of $125\,\mathrm{ns}$. However, it is not clear what would be the maximum time drift during a certain measurement interval.

In the present paper, a solution for the wireless characterization of large multi-port systems is proposed. A brief introduction to measurements with traditional VNAs is given in Section II. The baseband Wireless Vector Network Analyzer

Manuscript received Month xx, 2xxx. (Corresponding author: Markeljan Fishta.)

The authors are with the Department of Electronics and Telecommunication, Politecnico di Torino, 10129 Torino, Italy (e-mail: markeljan.fishta@polito.it, erica.raviola@polito.it, franco.fiori@polito.it).

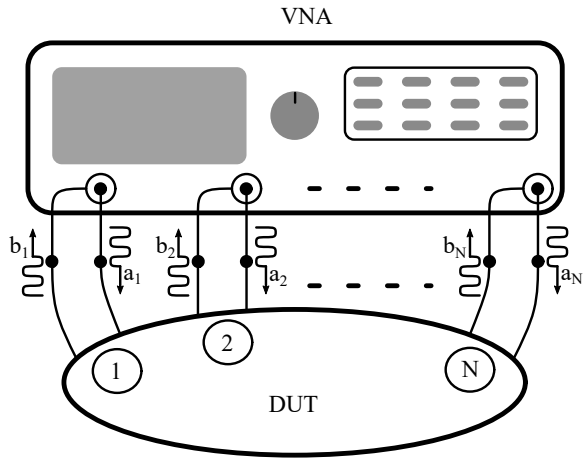

Fig. 1. Schematic representation of a DUT connected to a VNA. The DUT is generic and has N ports, as does the VNA.

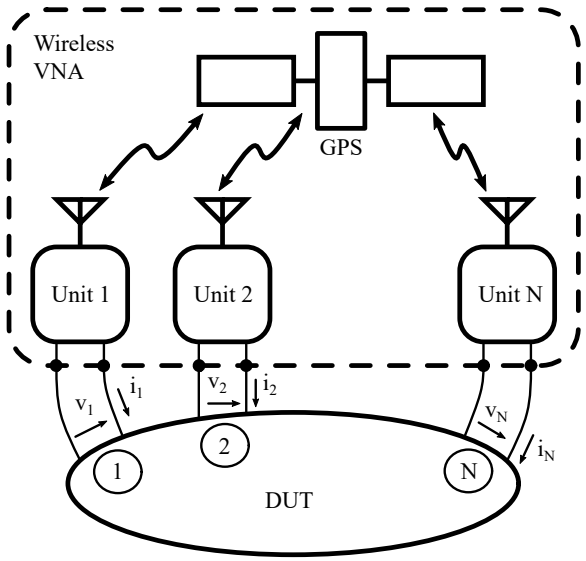

Fig. 2. Wireless frequency characterization system. The ports of the DUT are not wired among them.

(WVNA), well suited for the characterization of spatially large systems, is presented in Section III. The proposed method allows for a full characterization of multi-port devices. The contribution of the present work covers the hardware and software implementation, and the system validation, which is presented in Section IV. Finally, an application of the system to the characterization of water pipelines, used as an acoustic communication channel is presented in Section V. The paper is concluded in Section VI.

II. VNA OVERVIEW

A linear N port device can be represented and fully described by a NxN matrix, as seen from its ports. It is possible to employ different matrices, relating the various physical quantities at the ports. At microwave frequencies it is common to use the scattering matrix, which relates the incident with the reflected power waves at the ports. The instrument used for the measurement of such a matrix is a VNA [16]. A schematic representation of a VNA connected to a Device Under Test (DUT) is shown in Fig. 1. The incident and reflected power waves at each port are a_{i} and b_{i}, respectively, where i stands for the port index. The relation of the power waves by the scattering matrix can be expressed as [17]

$$\begin{bmatrix} b_1 \\ b_2 \\ \vdots \\ b_N \end{bmatrix} = \begin{bmatrix} s_{11} & s_{12} & \cdots & s_{1N} \\ s_{21} & s_{22} & \cdots & s_{2N} \\ \vdots & \vdots & \ddots & \vdots \\ s_{N1} & s_{N2} & \cdots & s_{NN} \end{bmatrix} \begin{bmatrix} a_1 \\ a_2 \\ \vdots \\ a_N \end{bmatrix}. \tag{1}$$

Each element of the matrix can be formally expressed as

$$s_{\mathrm{ij}} = \left. \frac{b_{\mathrm{i}}}{a_{\mathrm{j}}} \right|_{a_{\mathrm{k}}=0, k\neq j}, \tag{2}$$

which means that, when performing measurements between ports i and j, the other ports have to be matched, in order to null the incident waves on all ports except the jth. The incident wave at the jth port is the system excitation and it is generated by the VNA. The reason the VNA measures scattering matrices is that at microwave frequencies power waves can be measured easily [17]. However, scattering parameters can be converted into impedance or admittance ones.

III. PROPOSED METHOD

In order to be able to perform impedance characterization of large-scale structures, it is desirable to carry out measurements without wiring the ports of the DUT to the central unit. The idea behind the proposed system is presented in Fig. 2. The resulting measurement system is distributed, in which identical units are connected to the ports of the network to be characterized. The proposed system replicates the architecture of a traditional VNA, with the important distinction that the ports are not wired to one another.

As was previously said, a classical VNA measures incident and reflected waves at the ports. However, at lower frequencies, voltages and currents can be measured instead, so that the DUT can be characterized in terms of impedance or admittance matrices. The impedance matrix of the multi-port completely describes the system as seen at the ports, relating port quantities in a similar fashion to the scattering matrix.

$$\begin{bmatrix} v_1 \\ v_2 \\ \vdots \\ v_N \end{bmatrix} = \begin{bmatrix} z_{11} & z_{12} & \cdots & z_{1N} \\ z_{21} & z_{22} & \cdots & z_{2N} \\ \vdots & \vdots & \ddots & \vdots \\ z_{N1} & z_{N2} & \cdots & z_{NN} \end{bmatrix} \begin{bmatrix} i_1 \\ i_2 \\ \vdots \\ i_N \end{bmatrix}. \tag{3}$$

The choice of the representation depends on the DUT and on the easiest port termination to be realized, whether short circuit or open circuit. In order to perform synchronous signal acquisition at the ports, the present paper proposes the synthesis of the local clocks, used for the signal sampling among units, from a common reference source. In particular, an eligible signal for this task is the 1PPS reference clock, due to its high accuracy. This is a signal provided by some Global Navigation Satellite System (GNSS) receivers, which has a period of $1\,\mathrm{s}$ and period standard deviation of the order of $10\,\mathrm{ns}$, depending on the device generating the signal [18]. Using GPS, time comparisons can be performed with an accuracy of a few nanoseconds for short baselines ($1000\,\mathrm{km}$) and up to $20\,\mathrm{ns}$ for intercontinental distances [19]. Furthermore, the GPS signal

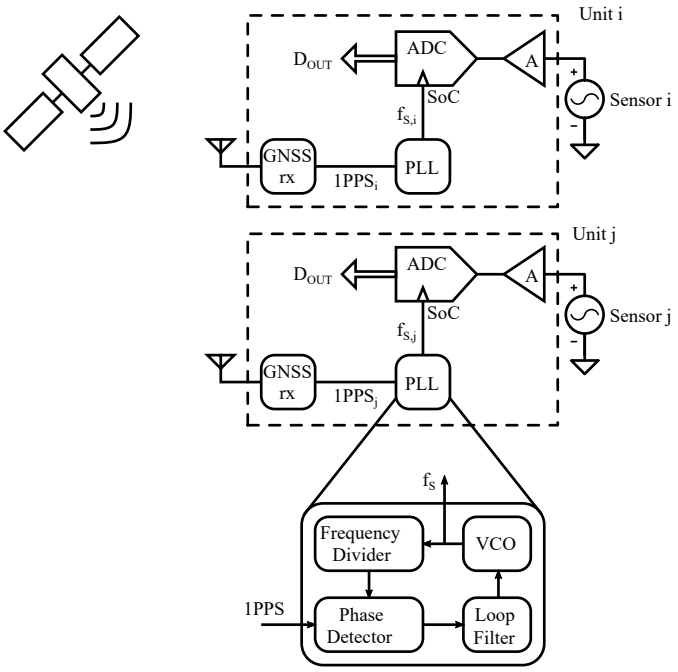

Fig. 3. Sampling clock synchronization mechanism among units i and j.

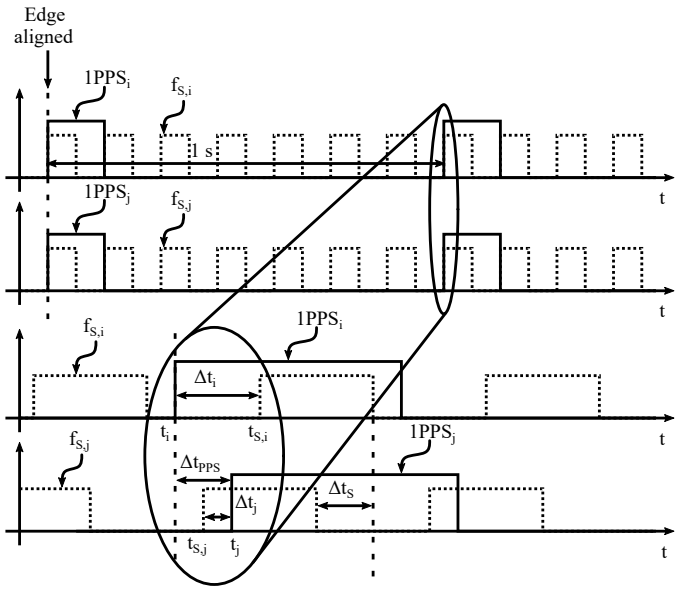

Fig. 4. Illustration of the effect of errors on timing signals among two units.

is widely available, even in remote areas, without requiring any dedicated infrastructure. In the proposed method, all the units at the ports of the WVNA receive the 1PPS signal, and local sampling clocks are synthesized by means of a Phase-Locked-Loop (PLL), as shown by the block diagram in Fig. 3. Focusing on the i-th unit, the PLL provides a sampling clock signal with frequency

$$f_{\mathrm{S,i}} = M f_{\mathrm{PPS,i}} \tag{4}$$

where M is a constant and $f_{\mathrm{PPS,i}}$ is the frequency of the 1PPS signal. Furthermore, the PLL enforces the phase lock between the reference signal and the synthesized clock signal, which results in

$$\Delta\varphi_{\mathrm{i,j}} = \varphi_{\mathrm{i}} - \varphi_{\mathrm{j}} = 0 \tag{5}$$

where φ denotes the phase of the sampling signal and the subscript indicates one of the units. This ensures that the generated clock signals have the same frequency and are edge locked across the units. The sensor sampling is then performed by using the synthesized clocks directly for the timing of the Analog to Digital Converters (ADCs), without any additional software or hardware layer, which avoids adding any uncertainty contributions.

A. Time Synchronization Analysis

The sampling clock signal generated as described earlier, deviates from the intended behavior due to non idealities of various components of the system, which include

- jitter of the reference signal from the GNSS module,
- additive jitter due to internal blocks of the PLL.

The effect of these errors onto the timing signals is illustrated in Fig. 4. The reference signal, generated by the GNSS module is ideally the same among all units. However, the pulse edge is affected by uncertainty giving rise to the time difference

$$\Delta t_{\mathrm{PPS}} = t_{\mathrm{j}} - t_{\mathrm{i}} \tag{6}$$

Furthermore, the edge of the clock signal of each unit will deviate from the edge of the reference signal of the respective unit. This is due to the phase noise and other non idealities in the PLL. The time difference between the edge of the clock signal and the PPS signal, for units i and j is given by

$$\Delta t_{\mathrm{i}} = t_{\mathrm{S,i}} - t_{\mathrm{i}}, \tag{7}$$

$$\Delta t_{\mathrm{j}} = t_{\mathrm{S,j}} - t_{\mathrm{j}}. \tag{8}$$

The phase error in the measurement of the transfer functions is related to the time difference between the pulse edges of the two clock signals, which is given by

$$\Delta t_{\mathrm{S}} = t_{\mathrm{S,j}} - t_{\mathrm{S,i}} = \Delta t_{\mathrm{j}} - \Delta t_{\mathrm{i}} + \Delta t_{\mathrm{PPS}}. \tag{9}$$

The accuracy of the 1PPS signal depends on the device that generates the signal. Jitter at the output of each PLL, on the other hand, depends both on the reference signal as well as the internal blocks of the PLL. Due to the complex internal structure of the employed PLL [20], an experimental approach was chosen for the evaluation of the clock jitter, and the results are provided in Section IV-B.

B. Hardware System Description

Although the focus was previously placed on the synchronous acquisition of the signals, the proposed method is meant to provide a way for exciting the structure under test. So, the units of which the system is composed contain a signal generation chain as well. A block diagram of the unit is represented in Fig. 5. As shown, the main subsystems are the elaboration unit (EU), the signal generation chain, signal acquisition chain and the synchronization module. Each unit communicates with a PC through a serial interface for the

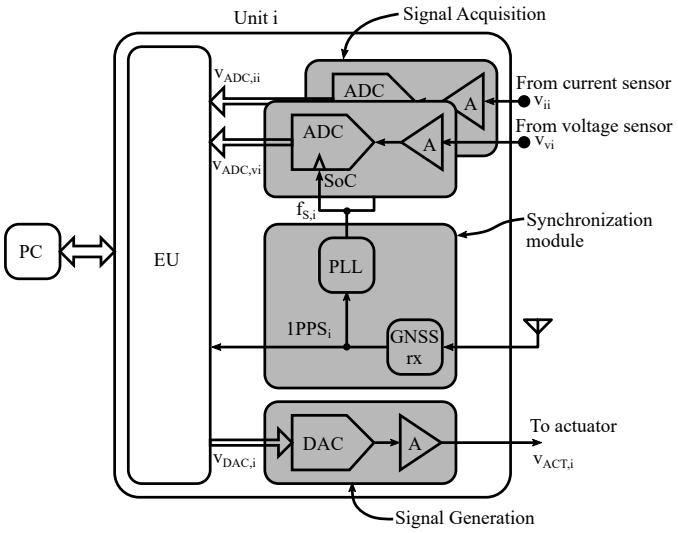

Fig. 5. Block diagram of the unit.

exchange of data. Data from all units are stored in a shared location, for later processing. Units are programmable and can be configured as active ports of the WVNA, providing the excitation signal to the structure under test, or as passive ports of the WVNA, which only perform monitoring of the response.

1) Elaboration Unit: The EU governs the characterization procedure by correctly timing the signal generation and signal acquisition operations. It consists of an ARM Cortex-M4-based microcontroller (uC), running off a $64\,\mathrm{MHz}$ crystal oscillator. Internal memory of $64\,\mathrm{kB}$ is used to temporarily store measurement results, before transferring them to a PC.

2) Signal Generation Chain: The proposed system makes use of a unit, which acts as the stimulus generator, to excite the system under examination. This is achieved by a suitable actuator, driven by the the signal generation chain. The excitation signal is synthesized, in digital form, on board the uC. This signal, $v_{\mathrm{DAC}}[n]$, is then applied to the Digital to Analog Converter (DAC) and after suitable conditioning the signal $v_{\mathrm{ACT}}(t)$ is obtained, which can be applied to the transducer exciting the structure.

3) Signal Acquisition Chain: The unit contains two signal acquisition chains, in order to measure two quantities at each port. It has to be remarked that the transducers are not part of the unit, but are added externally. This gives the proposed system the capability of characterizing different kinds of systems, such as electrical, mechanical and acoustic, by simply swapping the transducers. Each signal acquisition chain consists of a signal conditioning block, elaborating the signal from the transducer $v_{\mathrm{v}}(t)$ or $v_{\mathrm{i}}(t)$, and an ADC with a dedicated Start-of-Conversion (SoC) pin. The gain of the signal conditioning block is programmable from the uC. The ADC can operate with a maximum clock frequency of $500\,\mathrm{kSa/s}$ and has 16 bit resolution. After conversion, the digitized signal $v_{\mathrm{ADC}}[n]$ is obtained and stored in the RAM of the uC.

4) Synchronization Module: The employed synchronization scheme is hardware-based and it makes use of a low cost GSM/GNSS receiver [21], which can exploit multiple constellations such as GPS, GLONASS, Galileo, BeiDou and QZSS. The receiver provides absolute time stamps with a resolution of one second, besides the 1PPS signal. A Digital PLL (DPLL) block is used to provide the sampling clock signal, which is edge-locked to the reference signal, to the ADC. The 1 PPS signal is also connected to a General Purpose Input Output (GPIO) pin of the uC and acts as the clock for the software Finite State Machine (FSM) which cadences the operation of the system. The DPLL can operate from a minimum input frequency of $1\,\mathrm{Hz}$ and its parameters such as the loop bandwidth and the frequency division factor are programmable.

C. Proposed Characterization Procedure

Having described the hardware components, the characterization procedure, which can be divided into three phases, is detailed in what follows.

1) Unit Configuration: The first phase of the procedure deals with the initial configuration of the unit. The user chooses whether the unit should operate in the active or in the passive mode. Also, in this phase, the acquisition sampling frequency f_S and number of samples R are defined. The characterization procedure consists of a frequency sweep in which a sinusoidal signal is applied to the actuator, so an array of frequencies to be scanned along with an array of amplitudes are input from the user. Gains of the conditioning blocks are also set in this phase and all the components belonging to the subsystems shown in Fig. 5 are initialized. Of particular importance is the GNSS receiver. While the 1PPS signal is used to generate synchronized local clocks among the units, different units must be able to start the characterization procedure at the same time instant. This is achieved by using the absolute time stamps provided by the receiver. The user chooses the $targetTime$, meaning the local time in the format *hh:mm:ss*, at which the units will begin the characterization procedure. The DPLL module is initialized and configured in order to get at its output the desired clock frequency for the signal sampling. The lock status of the DPLL is periodically checked and, when achieved, the Unit Configuration phase is concluded.

2) Frequency Sweep: The frequency sweep procedure is implemented as a software Finite State Machine (FSM), whose state transition graph is shown in Fig. 6. Transitions among states are triggered by the edge of the 1PPS signal, which ensures the FSMs on two different units evolve synchronously through the state graph. At the beginning, the "Wait" state is entered, in which the units periodically compare $targetTime$ against the absolute time provided by the GPS. When $targetTime$ is reached, the FSM transits to the "Reset" state. Here, all the necessary variables are initialized. At the following 1PPS edge the state "Prepare" is reached, where the frequency index is updated. Also, if the unit is configured as active, the excitation signal is computed and stored. In the following state, "Acquire", if the unit is an active one, the signal generation is started. Also, for all units, the acquisition from the external ADC is started. Depending on the sampling

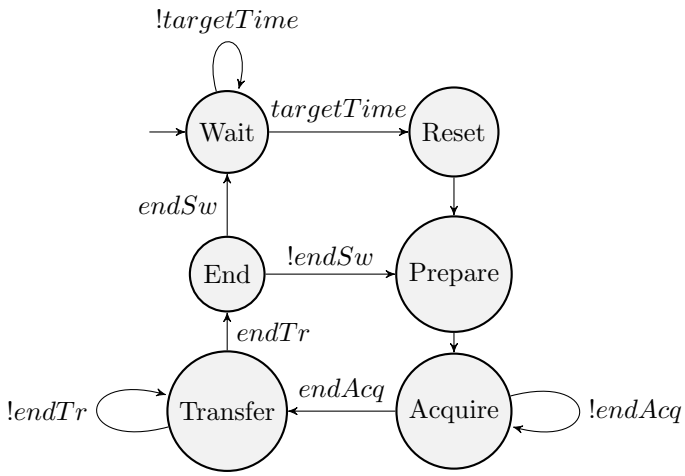

Fig. 6. State Diagram of FSM governing the frequency sweep procedure.

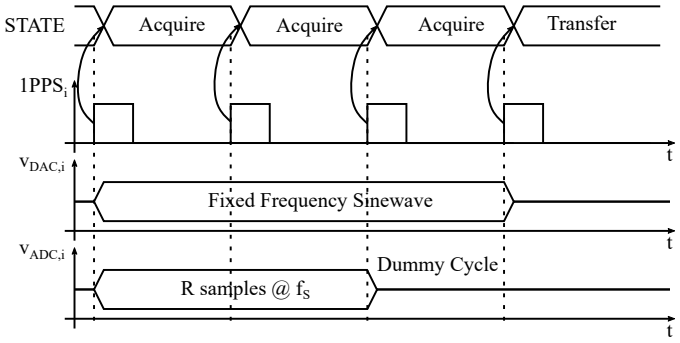

Fig. 7. Timing of the signal acquisition and generation in a unit. A case $q = 3$ has been assumed.

frequency f_{S} and on the number of samples R, the FSM remains in that state for a number of cycles

$$q = \frac{R/f_{\mathrm{S}}}{1\,\mathrm{s}} + 1, \tag{10}$$

at the end of which, the $endAcq$ signal is asserted. The additional cycle is introduced in order to allow for the correct alignment of FSMs on two different units, in case the acquisition ends exactly on the edge of the 1 PPS signal. In the end, R samples from the ADC have been stored in RAM so the signal generation is interrupted. The timing of signal generation and signal acquisition, covering the state "Acquire", is shown in Fig. 7, which refers to $q = 3$. The next state, "Transfer", is used for sending the acquired samples to a PC through the serial interface. The operation takes m cycles, at the end of which the $endTr$ signal is asserted and the next state is entered. In the "End" state, the frequency index is checked to verify whether the TF measurement procedure has ended, and the $endSw$ signal is set accordingly.

3) Post elaboration: After data acquisition and storage, the elements of the matrix of interest can be computed. In the present case a frequency-domain approach is adopted for the computation of the complex elements, by using the FFT (Fast Fourier Transform). For the sake of clarity, the computation will be illustrated by considering a two-port acoustic DUT.

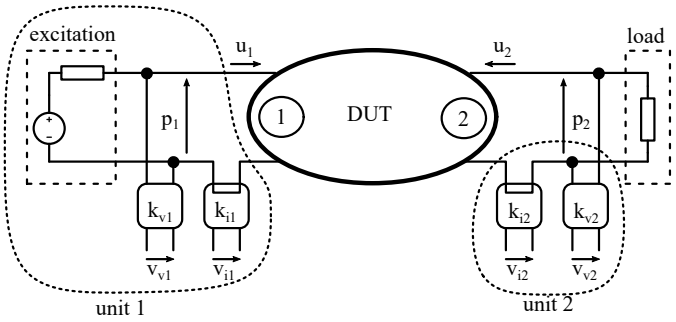

Fig. 8. Example of characterization of acoustic DUT. Only the relevant transducers are shown for each unit.

When dealing with mechanical or acoustic systems, analogies with electrical circuits are often used [22]. Voltage and current map into force and velocity for mechanical systems and into pressure and flux of fluid for acoustic systems, respectively. In the diagram of Fig. 8, the DUT connected to the transducers of two units is represented. In the schematic, p indicates pressure while u indicates flux of fluid at the port. Excitation to the system is provided at port 1, where the Thévenin model represents the actuator driven by Unit 1. At each port, two transducers are represented, measuring both pressure and flux of fluid and providing voltage outputs. If the structure is loaded in such a way that $u_2 = 0$, then $v_{\mathrm{i}2} = 0$ and the voltages $v_{\mathrm{v}1}$, $v_{\mathrm{v}2}$ and $v_{\mathrm{i}1}$ can be acquired. Each discrete-time domain voltage $v[r]$, with $r \in (0, 1, 2, ..., R-1)$ the discrete-time index, is transformed into the frequency-domain sample array

$$V[k] = \sum_{r=0}^{R-1} v[n] \cdot e^{-\jmath\frac{2\pi}{R}kr} \tag{11}$$

where $k \in (0, 1, 2, ..., R-1)$ is the discrete-frequency index. The frequency-domain evaluation of the signal allows one to consider only the component at the frequency of interest, i.e. the one which has been excited by the actuator. Two elements of the matrix describing the system can be computed

$$h_{11} = \left.\frac{V_{\mathrm{v}1}}{V_{\mathrm{i}1}}\right|_{V_{\mathrm{i}2}=0} \tag{12}$$

$$h_{21} = \left.\frac{V_{\mathrm{v}2}}{V_{\mathrm{i}1}}\right|_{V_{\mathrm{i}2}=0}. \tag{13}$$

By reversing the ports, applying the excitation to port 2 and loading port 1 such that $v_{\mathrm{i}1} = 0$, the other two elements of the matrix can be computed. In the end, a matrix H is obtained, relating the four voltages at the two ports

$$\begin{bmatrix} V_{v1} \\ V_{v2} \end{bmatrix} = \begin{bmatrix} h_{11} & h_{12} \\ h_{21} & h_{22} \end{bmatrix} \begin{bmatrix} V_{i1} \\ V_{i2} \end{bmatrix} = [H] \begin{bmatrix} V_{i1} \\ V_{i2} \end{bmatrix}. \tag{14}$$

The obtained matrix describes the system as seen from the measurement ports, hence it includes the DUT and the employed transducers. Next, the procedure for removing the effect of the transducers will be described.

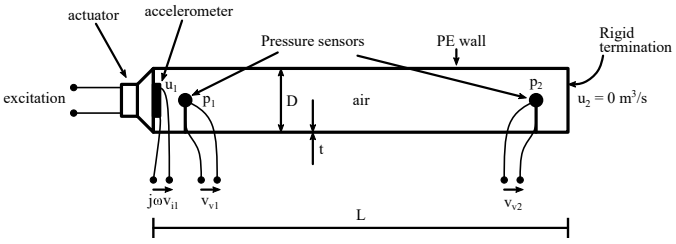

Fig. 9. Bench setup for the characterization of an acoustic device. A section view of the pipe is shown.

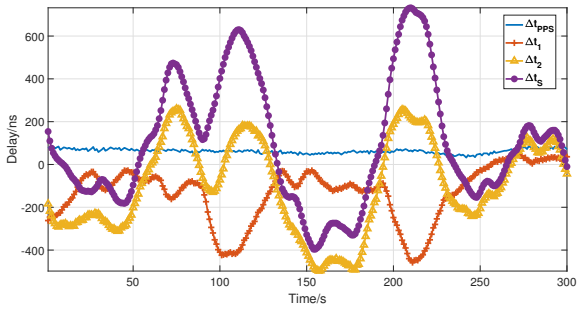

Fig. 10. Experimental characterization of the error in the timing signals. Delay times were measured by means of a digital oscilloscope.

D. Calibration

During the characterization procedure, unwanted error networks can be present. The procedure of their removal is known as calibration and it allows one to obtain the matrix of the DUT. In classic VNA measurements these error networks are commonly constituted by the connections between the ports of the VNA and those of the DUT. The procedure can be performed if the matrices describing the error networks are known [17]. The calibration problem will be discussed hereinafter for the case of characterization of the acoustic DUT, which is represented in Fig. 8. Having mapped the acoustic quantities into electrical ones, by analogy, the DUT can be described by the matrix of acoustic impedances, relating the port pressures to the fluid fluxes, as

$$\begin{bmatrix} P_1 \\ P_2 \end{bmatrix} = \begin{bmatrix} z_{a,11} & z_{a,12} \\ z_{a,21} & z_{a,22} \end{bmatrix} \begin{bmatrix} U_1 \\ U_2 \end{bmatrix} = \left[Z_\mathrm{a}\right] \begin{bmatrix} U_1 \\ U_2 \end{bmatrix} \tag{15}$$

where P and U are the frequency domain representation of the port pressure and flux of fluid, respectively. By knowing the conversion factor of the transducers, the impedance matrix of interest can be derived from the measured matrix $[H]$. By employing the transducer relations

$$V_\mathrm{v1} = k_\mathrm{v1} P_1 \tag{16}$$
$$V_\mathrm{v2} = k_\mathrm{v2} P_2 \tag{17}$$
$$V_\mathrm{i1} = k_\mathrm{i1} U_1 \tag{18}$$
$$V_\mathrm{i2} = k_\mathrm{i2} U_2, \tag{19}$$

it results

$$\left[Z_\mathrm{a}\right] = \begin{bmatrix} k_{v1} & 0 \\ 0 & k_{v2} \end{bmatrix}^{-1} [H] \begin{bmatrix} k_{i1} & 0 \\ 0 & k_{i2} \end{bmatrix}. \tag{20}$$

Therefore, the contribution due to the components that do not belong to the DUT is removed.

IV. System Validation

Experimental measurements were performed in order to assess the time error on the edge of the clock signals and validate the proposed system, by comparison with a traditional wired one.

A. Test Bench

The validation test bench is shown in Fig. 9. The chosen acoustic DUT was a ployethylene pipe segment, with internal diameter of $D = 69\,\mathrm{mm}$, wall thickness $t = 10.5\,\mathrm{mm}$ and length $L = 1\,\mathrm{m}$. The actuator used with Unit 1 was an audio speaker. Port 2 was terminated with a rigid surface in order to accomplish the load condition $u_2 = 0$, required for the measurement of impedance elements related to port 1. The pressure sensors at the two ports were two microphones with sensitivity $k_\mathrm{v1,2} = 10\,\mathrm{mV/Pa}$ while acceleration of the air particles was measured in order to indirectly evaluate the flux of fluid at port 1. This was accomplished by means of an accelerometer with sensitivity $k_\mathrm{acc} = 31\,\mathrm{mV/(m/s^2)}$, which was integral to the speaker cone. The flux of fluid, which is the quantity of interest, can be evaluated from the acceleration as

$$U_1 = A \frac{a_1}{\jmath 2\pi f}, \tag{21}$$

resulting in the transduction factor

$$k_\mathrm{i1} = \frac{k_\mathrm{acc} \cdot \jmath 2\pi f}{A} \tag{22}$$

where a_1 is air acceleration, f is the excitation frequency and A is the internal area of the pipe cross section.

B. Clock synchronization quality assessment

Repeated measurements of the time jitter between two units were carried out in order to evaluate the statistical properties of such jitter. Fig. 10 shows the results of 300 measurements on the time interval occurring between the different reference timing signals. The DPLL blocks were configured so that the loop bandwidth was

$$f_\mathrm{PLL} = 50\,\mathrm{mHz}, \tag{23}$$

which, assuming $\zeta = \frac{\sqrt{2}}{2}$, corresponds to a natural frequency [23]

$$\omega_\mathrm{n} = \frac{2\pi f_\mathrm{PLL}}{2.1} = 150\,\mathrm{mrad/s} \tag{24}$$

and gives rise to a lock time of

$$t_\mathrm{lock} = \frac{6.02}{\omega_\mathrm{n}} = 40\,\mathrm{s}. \tag{25}$$

One time delay measurement was taken at each 1PPS edge, so the measurement interval was 300 s. It resulted that the time delay between the two 1PPS signals had mean value and variance

$$\overline{\Delta t_\mathrm{PPS}} = 62.3\,\mathrm{ns} \tag{26}$$

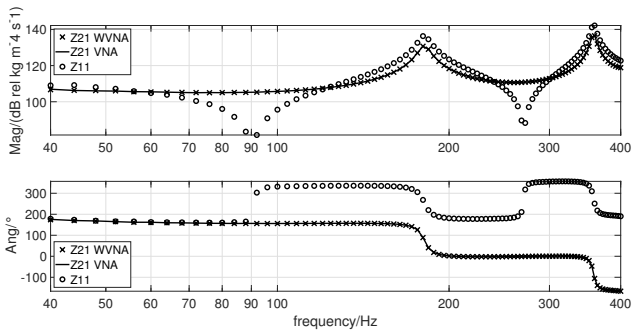

Fig. 11. Measurement results of acoustic device. Transfer impedance traces, measured with the two different methods, are overlapped.

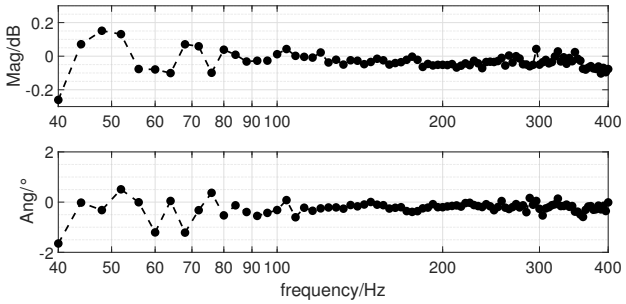

Fig. 12. Difference between the measurement of Z_{21} by means of the WVNA with respect to the VNA, in (top) magnitude $20\log|Z_{21,\mathrm{WVNA}}| - 20\log|Z_{21,\mathrm{VNA}}|$ and (bottom) phase $\angle Z_{21,\mathrm{WVNA}} - \angle Z_{21,\mathrm{VNA}}$.

$$\sigma_{\Delta t_{\mathrm{PPS}}} = 10.7\,\mathrm{ns} \tag{27}$$

while the same metrics for the two clock signals yielded

$$\overline{\Delta t_{\mathrm{S}}} = 98.2\,\mathrm{ns} \tag{28}$$

$$\sigma_{\Delta t_{\mathrm{S}}} = 290.4\,\mathrm{ns}. \tag{29}$$

The maximum variation over the observation interval was

$$\Delta t_{\mathrm{S,pp}} = 1.13\,\mu\mathrm{s}, \tag{30}$$

which can be used to estimate the maximum phase error in a certain frequency band.

C. Measurement results

Measurements on the acoustic device were carried out, with the aim to show the calibration procedure described earlier, as well as to compare the transfer impedance of a two-port system obtained with the proposed WVNA with that resulting from a traditional wired instrument. Assuming that the pipe segment is symmetrical, only characterization by excitation at port 1 was performed. A frequency range of $(40\,\mathrm{Hz}, 400\,\mathrm{Hz})$, with a frequency step $f_{\mathrm{STEP}} = 4\,\mathrm{Hz}$, was covered. The acoustic impedances were evaluated according to (20) obtaining the results shown in Fig. 11. Comparison of the transfer impedance measured with the proposed WVNA and a traditional wired VNA are in good agreement, showing maximum error fluctuation of $0.41\,\mathrm{dB}$ and $2.16°$ for the magnitude and phase, respectively, which are shown in Fig. 12.

V. Application Example

The proposed WVNA was used to characterize a guided acoustic wave channel. The system under consideration was a water distribution pipeline, in which two access points at a distance $L_{\mathrm{b}} = 73\,\mathrm{m}$ were identified. The pipe is buried in soil at a depth of around $1\,\mathrm{m}$ and it is meant to be used as a communication channel for an acoustic wave-based system. Hence the characterization of the channel is carried out using transducers from voltage to pressure and vice versa at the ports of the plant. A schematic representation of the characterization setup is shown in Fig. 13, while the main physical characteristics of the plant are given in Table I. At the access points, two units are mounted onto the pipe by means

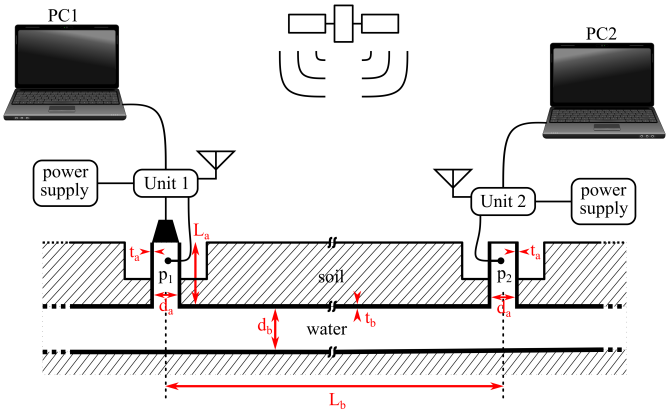

Fig. 13. Schematic representation of pipeline characterization setup. The main propagation path has length $L_{\mathrm{b}} = 73\,\mathrm{m}$ while the modules interface to the main pipe through two vertical pipe segments with length $L_{\mathrm{a}} = 1\,\mathrm{m}$.

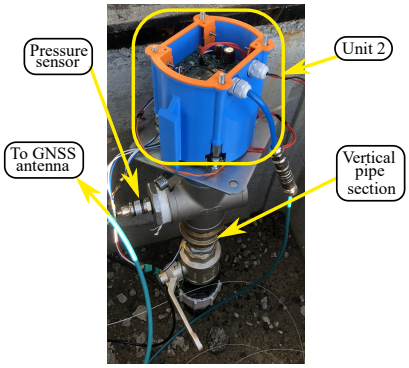

Fig. 14. One of the developed units attached to the communication channel to be characterized.

TABLE I
PHYSICAL PARAMETERS OF THE PIPELINE UNDER TEST.

Parameter	Value
Material	Polyethylene
L_{a}	$73\,\mathrm{m}$
L_{b}	$1\,\mathrm{m}$
d_{a}	$51.4\,\mathrm{mm}$
d_{b}	$90\,\mathrm{mm}$
t_{a}	$5.8\,\mathrm{mm}$
t_{b}	$10\,\mathrm{mm}$

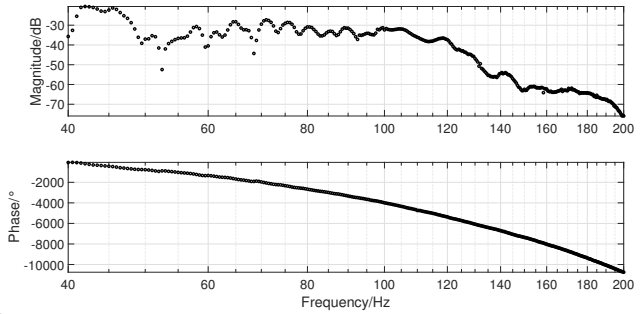

Fig. 15. Measurement result of the pressure transfer function $H(\jmath\omega)$.

of two vertical pipe segments approximately $1\,\mathrm{m}$ long. One of them is shown in Fig. 14. The aim of the characterization procedure is to assess the frequency dependent attenuation of pressure waves traveling inside the channel. Hence, voltages at the output of the pressure sensors were measured and the pressure transfer function was computed by taking the ratio

$$H(\jmath\omega) = \frac{P_2(\jmath\omega)}{P_1(\jmath\omega)} = \frac{V_{\mathrm{v}2}(\jmath\omega)}{V_{\mathrm{v}1}(\jmath\omega)} \cdot \frac{k_{\mathrm{v}1}}{k_{\mathrm{v}2}}. \tag{31}$$

A frequency range $(f_{\mathrm{MIN}}, f_{\mathrm{MAX}}) = (40\,\mathrm{Hz}, 200\,\mathrm{Hz})$ was chosen, with a frequency step of $f_{\mathrm{STEP}} = 0.5\,\mathrm{Hz}$, in order to enable the observation of the frequency selectivity of the channel. The chosen frequency step corresponds to an acquisition time

$$t_{\mathrm{ACQ}} = \frac{1}{\Delta f} = 2\,\mathrm{s}. \tag{32}$$

The results are plotted in Fig. 15. They showed a non flat magnitude response, with several deep notches, and a phase angle increasing with frequency. The measurements are useful for the selection of the carrier frequency, which should be far from the notches. Moreover, the measurement of the complex transfer function enables channel modeling by fitting techniques, for the simulation of the communication channel.

VI. Conclusion

A Wireless Vector Network Analyzer, designed for the frequency characterization of spatially large objects, was presented in this paper. The proposed system extends the concept of a traditional VNA by removing the requirement of wiring the ports of the device under test to the processing unit. For this purpose, a GPS-based synchronization scheme was developed, which allowed for synchronous signal acquisition at the ports of the system. This greatly simplified installation, making the system suitable for field applications. The work covered the hardware and software development, and experimental tests showed a phase error fluctuation of $2.16°$ in a measurement frequency range of $(40\,\mathrm{Hz}, 400\,\mathrm{Hz})$, by reducing jitter at $1.13\,\mu\mathrm{s}$ over a $300\,\mathrm{s}$ observation interval.

The proposed system can find application in communication channel characterization and in Transfer Impedance-based methods for Structural Health Monitoring. An application example was presented as well, in which a water distribution pipeline was characterized as an acoustic waveguide.

References

[1] K. M. Joseph, T. Watteyne, and B. Kerkez, "Awa: Using water distribution systems to transmit data: Awa: Using to Transmit Data," *Transactions on Emerging Telecommunications Technologies*, vol. 29, no. 1, p. e3219, Jan. 2018.

[2] L. Jing, Z. Li, Y. Li, and R. D. Murch, "Channel Characterization of Acoustic Waveguides Consisting of Straight Gas and Water Pipelines," *IEEE Access*, vol. 6, pp. 6807–6819, 2018.

[3] S. He, N. Wang, M. Ho, J. Zhu, and G. Song, "Design of a New Stress Wave Communication Method for Underwater Communication," *IEEE Transactions on Industrial Electronics*, vol. 68, no. 8, pp. 7370–7379, Aug. 2021.

[4] D. Wei, C. Qi, C. Huang, J. Chen, A. Song, G. Song, and M. Pan, "Riding Stress Wave: Underwater Communications Through Pipeline Networks," *IEEE Journal of Oceanic Engineering*, vol. 46, no. 4, pp. 1450–1462, Oct. 2021.

[5] M. Dziendzikowski, P. Niedbala, A. Kurnyta, K. Kowalczyk, and K. Dragan, "Structural Health Monitoring of a Composite Panel Based on PZT Sensors and a Transfer Impedance Framework," *Sensors*, vol. 18, no. 5, p. 1521, May 2018.

[6] V. Giurgiutiu, *Structural Health Monitoring with Piezoelectric Wafer Active Sensors*. Amsterdam: Academic Press, an imprint of Elsevier, 2014.

[7] W. K. Chiu, Y. L. Koh, S. C. Galea, and N. Rajic, "Smart structure application in bonded repairs," *Composite Structures*, vol. 50, no. 4, pp. 433–444, Dec. 2000.

[8] R. Mateusz, R. Mateusz, M. Adam, M. Adam, and U. Tadeusz, "An Overview of Electromechanical Impedance Method for Damage Detection in Mechanical Structures," p. 8.

[9] S. Bhalla, A. Gupta, S. Bansal, and T. Garg, "Ultra Low-cost Adaptations of Electro-mechanical Impedance Technique for Structural Health Monitoring," *Journal of Intelligent Material Systems and Structures*, vol. 20, no. 8, pp. 991–999, May 2009.

[10] L. M. Campeiro, R. Z. da Silveira, and F. G. Baptista, "Impedance-based damage detection under noise and vibration effects," *Structural Health Monitoring*, vol. 17, no. 3, pp. 654–667, May 2018.

[11] Z. Su and L. Ye, *Identification of Damage Using Lamb Waves: From Fundamentals to Applications*, ser. Lecture Notes in Applied and Computational Mechanics. Berlin: Springer, 2009, no. 48.

[12] C. R. Paul, *Introduction to Electromagnetic Compatibility*, 2nd ed., ser. Wiley Series in Microwave and Optical Engineering. Hoboken, N.J: Wiley-Interscience, 2006.

[13] A. B. Noel, A. Abdaoui, T. Elfouly, M. H. Ahmed, A. Badawy, and M. S. Shehata, "Structural Health Monitoring Using Wireless Sensor Networks: A Comprehensive Survey," *IEEE Communications Surveys & Tutorials*, vol. 19, no. 3, pp. 1403–1423, 2017.

[14] E. Sazonov, V. Krishnamurthy, and R. Schilling, "Wireless Intelligent Sensor and Actuator Network - A Scalable Platform for Time-synchronous Applications of Structural Health Monitoring," *Structural Health Monitoring*, vol. 9, no. 5, pp. 465–476, Sep. 2010.

[15] A. Araujo, J. Garcia-Palacios, J. Blesa, F. Tirado, E. Romero, A. Samartin, and O. Nieto-Taladriz, "Wireless Measurement System for Structural Health Monitoring With High Time-Synchronization Accuracy," *IEEE Transactions on Instrumentation and Measurement*, vol. 61, no. 3, pp. 801–810, Mar. 2012.

[16] Agilent Technologies, "Agilent E5061A/E5062A User's Guide," Sep. 2009.

[17] D. M. Pozar, *Microwave Engineering*, 4th ed. Hoboken, NJ: Wiley, 2012.

[18] X. Niu, K. Yan, T. Zhang, Q. Zhang, H. Zhang, and J. Liu, "Quality evaluation of the pulse per second (PPS) signals from commercial GNSS receivers," *GPS Solutions*, vol. 19, no. 1, pp. 141–150, Jan. 2015.

[19] W. Lewandowski and C. Thomas, "GPS time transfer," *Proceedings of the IEEE*, vol. 79, no. 7, pp. 991–1000, Jul. 1991.

[20] "AD9545 Datasheet and Product Info | Analog Devices." [Online]. Available: https://www.analog.com/en/products/ad9545.html

[21] "MC60 specification." [Online]. Available: https://www.quectel.com/wp-content/uploads/pdfupload/Quectel_MC60_GSM_Combo_Specification_V1.3.pdf

[22] L. L. Beranek, *Acoustics: Sound Fields, Transducers and Vibration*, 2nd ed. Canbridge, MA: Elsevier, 2019.

[23] B. Razavi, *RF Microelectronics*, 2nd ed. Upper Saddle River, NJ: Prentice Hall, 2012.